International Journal of Physical Modelling in Geotechnics

A novel experimental technique to model impression piles in centrifuge testing

PHMG-2022-065-R2 | Paper

Submitted on: 19-07-23

Submitted by: Leonardo Maria Lalicata,Eric Ritchie,Sarah Stallebrass,Andrew McNamara

Keywords: CENTRIFUGE MODELLING,CLAYS,IMPRESSION PILE,WORKING LOAD


RIVER VALLEY
TECHNOLOGIES

A novel experimental technique to model impression piles in centrifuge testing

Leonardo Maria Lalicata[1], Eric Ritchie[2], Sarah Elizabeth Stallebrass[2], Andrew McNamara[2]

1: University of Genoa

2: City, University of London

Corresponding author: Leonardo Maria Lalicata. leonardo.lalicata@unige.it

Abstract

A novel experimental technology for small scale centrifuge tests on piled foundations has been investigated. The technology is suitable for bored piles where the pile shaft has been profiled to improve the bearing capacity. One such pile is an impression pile that has an enhanced shaft capacity due to the small impressions created along the shaft. In previous centrifuge testing, impression piles have been created by pouring resin into a profiled bore. However, in the technique to be described a novel pile made of 3D printed rigid plastic with a reverse mandrel mechanism is used to create a nodular shaft surface during installation in the clay sample. Once assembled the pile has the same geometry as the cast *in situ* impression pile. Compared to the resin piles, 3D printed plastic piles allow for faster model making and demonstrate excellent repeatability. Because of the ductile behaviour of the soil-plastic interface it is possible to see how the impressions improve the performance of a pile over the whole load-settlement curve, not just at ultimate capacity. In addition, a greater percentage increase in ultimate capacity was registered for the 3D printed plastic impression piles compared to similar resin impression piles. The plastic-soil interface has an α value which is closer to that commonly encountered in the field. At working load, the 3D printed plastic impression piles outperformed traditional straight shafted piles by 90%.

Keywords: impression pile, working load, centrifuge modelling, clay, 'UN SDG 09'

Introduction

Deep foundations in centrifuge testing are typically modelled as solid metallic rods or tubes (Rollins *et al.*, 2005; Rosquoët *et al.*, 2007; Ng *et al.*, 2014; Alnuaim *et al.*, 2015; Lalicata *et al.*, 2019, 2020b; de Sanctis *et al.*, 2021; Li *et al.*, 2022, Shabanpour and Ghazavi, 2022), the latter having open or closed ends according to testing needs. These are extensively adopted owing to their cheap price, extensive availability on the market and ease of machining and assembling on often complex centrifuge packages. Metal model piles can reproduce the behaviour of prototype steel piles, such as monopiles for wind turbines, and they are also suitable for investigating installation effects (Truong *et al.*, 2019; Maatouk *et al.*, 2022; Li *et al.*, 2023). Recently, the use of rapid curing concrete piles in centrifuge tests is receiving increasingly interest, especially to capture the true failure mechanisms (Knappett *et al.*, 2011; Al-Dafae and Knappett, 2014; Goode and McCartney, 2015; Iovino *et al.*, 2023; Ouzzine *et al.*, 2023). Although rapid, these concrete piles need approximately one week of curing time in the mould before being installed in the soil models.

Therefore, such concrete model piles as well as metal model piles cannot be used, at least in clay samples, to model piles with an uneven cross-section along their length such as threaded/ribbed piles and impression piles (Hard & Carvalho, 2018; Gorasia and McNamara, 2016; Lalicata *et al.*, 2022, 2023). In those types of piles, the shaft capacity is enhanced by modifying the profile of the shaft. Ribbed piles are created with a tool that cuts concentric rings in the shaft, while in the impression pile the enhancement is provided by creating small discrete impressions that lead to a nodular pile surface. On site, once the profiling is concluded, the concrete is cast as in traditional bored piles. To reproduce such piles in physical model testing, polyurethane resin can be used (Chandler and Martins, 1982; McNamara *et al.*, 2009). Fast cast resin model piles have been extensively used at City, University of London in the past 20 years for a variety of problems, including investigations of settlement reduction associated with deep excavations (McNamara 2001, McNamara *et*

al., 2009), and the investigation of innovative pile foundations such as the aforementioned ribbed and impression piles (Taylor *et al.*, 2013; Gorasia and McNamara, 2016; Lalicata *et al.*,2023).

As with all modelling techniques, the use of polyurethane resin has drawbacks. The curing process seems to affect the soil-pile interface properties at small strain levels thus obscuring the effect of the enhanced shaft geometry of, for instance, ribbed piles. Gorasia and McNamara (2016) observed that ribbed piles with a ribbed length of 135mm (over 180mm total pile length) needed a large head displacement (from 5 to 10% of the diameter) to mobilise a significant increase in load compared to the plain pile, Figure 1. Moreover, for resin plain model piles, Lalicata *et al.* (2022) measured quite high values of the adhesion factor α, ~0.73, thus potentially compromising a direct comparison with field performances.

To address the limitations linked to the curing effects of resin, an alternative method to create model piles with profiled shafts has been developed. This is a model pile with a special sliding mechanism that allows the model pile to be inserted into the bore with the nodules retracted inside the pile and that, once the model pile is installed, subsequently pushes the nodules against the soil creating the impressions. This has been achieved using a model pile made of 3D printed rigid plastic components with a specially designed reverse mandrel mechanism. A number of small-scale centrifuge tests are reported to evaluate the performance of the plastic model piles and these are supported by interface direct shear tests. The behaviour of the 3D printed plastic model piles has been assessed against cast resin model piles by looking at the whole load-settlement curve, from small strain to ultimate capacity.

1. The impression pile

A sketch of the impression pile is illustrated in Figure 2a. In the simplest configuration, four nodules are impressed at a given cross section, spaced at 90º around the axis of the pile, and nodules are aligned in the vertical direction. Following Lalicata *et al*. (2023) the portion of the pile shaft where the impressions are created is called the active length L_a; s is the centre-to-centre vertical distance between two levels of nodules, n is the number of nodules at a given cross section and z is the position of the centre of the impressed zone relative to the soil surface. The geometry of the nodules is defined by the protruding length b, the width in the horizontal plane l and the vertical height h. In the centrifuge tests the nodules had a square cross section ($l = h$).

Lalicata *et al.* (2022, 2023) explored in greater detail the ultimate capacity of the impression pile by centrifuge testing on cast resin model piles and the topic will not be discussed here. For the purpose of this paper, it is recalled that the ultimate capacity of the impression pile increases with the active length and the number of nodules at a given horizon. Lalicata *et al.* (2023) demonstrated that the spacing s has little influence on the ultimate capacity of the impression piles when below a threshold value (s_{cr}), because the failure surface around the nodules bridges vertically, creating a vertical block of soil connecting adjacent nodules with the failure surface on the outside of this block, Figure 2b. In this configuration, the performance of the impression pile is maximised, i.e. there is a maximum increase in capacity compared to the straight shafted pile.

2. Experimental technique

Both 3D printed and resin piles are cored, profiled and installed in the centrifuge model at 1*g*. For results to be repeatable it is key that the piles are vertical, of constant length into the clay and the profiling of the impressions is precisely located and well defined. The piles were 16mm in diameter; embedded 180mm into the clay model.

The pile bores were cut using a hypodermic thin-walled tube with an external diameter of 16mm. The tube was mounted onto a brass handle to allow for easy cutting. The verticality and position of the piles was achieved using a system of guides (Lalicata *et al.*, 2020b). To minimise soil disturbance during boring, several precautions were taken: the internal part of the tube was sprayed with a lubricant oil and the edge of the tube was sharpened. In addition, the excavation of the bore was always undertaken in three steps of equal length.

2.1. Resin Model Pile

After profiling, the model piles were cast using a 'fast cast' polyurethane resin, Sika Biresin G27 (McNamara, 2001; McNamara and Taylor, 2002). The pot life of the resin was approximately 3 minutes. Aluminium powder was used as filler in an equal mass ratio with the two components of the resin to ensure that the model pile was not buoyant. The mixture was designed to have a good fluidity to fill the small impressions (1.5 x 1.5 x 3 mm). An aluminium collar placed on the top of the model pile accommodated the loading and measurement equipment.

The model impression piles were created from the plain pile bore. A custom designed tool was inserted into the guide and used to profile the pile bore, Figure 3. Figure 4a shows some of the exhumed model piles and demonstrates the success of this methodology. Several uniaxial compression tests were undertaken to measure the mechanical properties of the resin when set. The resin was found to have a Young's Modulus equal to 1.1 GPa and a yield stress of 35 MPa.

2.2. 3D Printed Model Pile

Figure 4b shows the assembled model piles that were made from a rigid 3D printed plastic, for simplicity referred to as plastic model piles in the following. The model pile is made from a central core with eight guiding rails along which eight segmental plates can slide during the installation process, Figure 5. Four plates have a curved but smooth external surface and

the other four house the nodules. During installation the plates are supported by a circular base 10mm thick with 20mm long guides. On the central core, the rails where the plates with nodules slide are slightly tapered to ensure that the nodules are fully retracted during insertion of the pile in the smooth sided bore. Once the pile is fully inserted into the bore, the core is manually pushed down, and the tapered profile of the rails makes the nodules expand into the soil, Figure 5b and Figure 6. The core is specifically machined to allow for easy handling and to accommodate the loading and measurement equipment. Several uniaxial compression tests were undertaken to measure the mechanical properties of the assembled plastic model pile. The plastic model pile was found to have a Young's Modulus equal to 0.75 GPa which is lower than the Young's Modulus of the material (2.2 GPa), declared by the manufacturer, the yield stress is equal to 55 MPa.

2.3. Soil

The Speswhite Kaolin clay used in the tests was prepared from slurry with an initial water content of approximately 120%; which is twice the liquid limit. The slurry was created by mixing dry powder and distilled water in an industrial ribbon blade mixer.

The slurry was carefully placed into the model container and manually agitated to expel the main air bubbles. The inside faces of the model container had been previously coated with water pump grease to minimise friction at the boundaries (Philipps, 1995). Beneath the slurry there was a filter paper and a 3 mm porous plastic sheet, with an aluminium drainage plate at the base. On top of the slurry, a second filter paper and porous plastic sheet were placed and drainage was allowed through holes in a loading platen. Consolidation pressure was applied in increments by means of a hydraulic press over a period of 9 days including 1 day of swelling. Following Taylor *et al.* (2013) and Gorasia and McNamara (2016) the maximum pressure was maintained for three days at which stage all measurable settlement had ceased. The samples were compressed to a vertical stress of 500kPa that was then reduced to 250kPa, producing a firm, but still workable, clay sample (McNamara *et al.*, 2009; Divall

and Goodey, 2015). On the day of the test, the sample was removed from the press and prepared for the centrifuge test, as described below.

3. Methodology

The performance under axial loading of the novel plastic model impression piles is assessed against that of cast resin model impression piles via centrifuge testing undertaken at 50*g* using a homogeneous overconsolidated clay deposit. In each experiment, the model impression piles were tested alongside a plain, straight shafted model pile of the same type (i.e. plastic or cast resin) to provide a baseline response for comparison purposes. The friction at the material-soil interface is further investigated by direct shear box testing for both the resin and plastic.

3.1. Layout of the Centrifuge tests

The Geotechnical Engineering Research Group at City, University of London, makes use of an Acutronic 661 beam centrifuge of 1.8m radius from centre to the swinging platform, described in detail by Schofield and Taylor (1988). The package containing the model was installed on the centrifuge once the piles had been bored, installed and the loading apparatus assembled on the plane strain strongbox. The whole process; removing the sample from the press to spin up, took approximately 2 hours. Once placed on the centrifuge swing, the model was accelerated to 50*g*.

During flight, the water table was maintained at a depth of approximately 10 mm below ground level by means of a constant head standpipe connected to the bottom of the model. The top surface was sealed with a sprayed synthetic rubber coating to prevent clay drying during the test; once dried this was only ~400 μm thick and it is known to not influence soil settlements (Le and Taylor, 2018). The model was left at 50*g* for about 48 hours until conditions of pore pressure equilibrium were established as identified by pore pressure

149 transducers embedded in the soil and one LVDT placed at the ground surface. The piles
150 were then loaded until failure at a displacement rate of 1mm/min.

151 For each test, the soil sample provided up to four testing sites within the rectangular
152 strongbox, Figure 7. The piles were positioned on the centreline of the model, 100 mm from
153 the sides, which was far enough to minimise boundary effects (Phillips, 1995). The piles
154 were spaced 110 mm or 165mm apart for the four or three pile configurations respectively
155 and loaded simultaneously by means of a very stiff beam connected to a lead screw and
156 motor. The apparatus was devised so that it was possible to obtain independent load and
157 settlement data for each pile. Three load cells, each of 5kN capacity, sandwiched between
158 two aluminium plates, measured the load on each pile ensuring that errors due to bending in
159 the load cell are eliminated, Figure 7. A ball bearing lying on top of a concave plate was
160 used to apply the centred and vertical load. A 2 mm thick aluminium plate, 175 mm long and
161 16 mm wide, was a tight fit to the pile collar and two LVDTs measure the plate displacement
162 at its extremes. The head displacement of the pile was given by the mean value of the LVDT
163 measurements. A 1 mm gap between the plate and the concave dish guaranteed that load
164 and displacement were independent readings. Additional details of the experimental
165 arrangement are given in Lalicata *et al.* (2020b).

166 *Soil characterisation*

167 Following testing on the centrifuge, the undrained shear strength was estimated from hand
168 vane tests and water content samples as in Lalicata *et al.* (2023). The soil strength
169 measurements for the tests given in Figure 8a are for the values derived from water
170 contents, via eq (1), where T12, T13 etc are the test names.

$$s_u = \frac{1}{2} M e^{\frac{(\Gamma - v)}{\lambda}} \quad (1)$$

where *v* is the specific volume the values of the parameters and their meaning are listed in Table 1. Note that, under fully saturated conditions, water content *w* and specific volume *v* are uniquely correlated: $v = 1 + wG_s$.

The measurements are largely consistent across all tests and in good agreement with the previous experiments (Lalicata *et al.*, 2023). As might be expected, the undrained strength increased slightly with depth. The data are generally inside the 10% error band with respect to the best fit line:

$$s_{u,w} = 41.2 + 0.044z \quad (2)$$

where $s_{u,w}$ is expressed in kPa and *z*, in mm, is the soil depth at the model scale. The profile of overconsolidation ratio (OCR), with depth for the tests is reported in Figure 8b.

3.2. Direct shear tests

Tests are performed on square samples (100x100mm) under a constant vertical stress of 50kPa, and a displacement rate of 1mm/min in a sealed box with no water, to avoid changes in the water content and to ensure *"undrained conditions"*. Although this is not the standard procedure for direct shear tests in clay, this methodology provides a reasonable approximation to the loading conditions in the centrifuge tests. The results should, however, be seen only as qualitative and treated with caution. The undrained shear strength is calculated from the water content measurements taken before and after each test.

The soil samples are cut from a lump of clay one dimensionally consolidated in a CBR mould to 500kPa and then unloaded to 250kPa, to give a similar loading history to that employed in the centrifuge tests. Except in the tests where resin was cast against the clay, soil samples were prepared and tested within 20 minutes, minimising any change in water content during testing and no change in water content was observed.

193 Four types of tests have been investigated:

194 • clay-clay test: standard direct shear test for reference.
195 • resin-clay test: the clay occupies only the lower half of the shear box; the top of the
196 clay was carefully trimmed to the level of the shear plane. Once the shear box was
197 assembled, the resin was poured against the clay surface to form a uniform layer
198 4mm thick. The resin was left curing for one hour with the top exposed to the air in a
199 temperature-controlled room before the test began.
200 • pre-cast resin-clay test: the clay occupies only the lower half of the shear box and a
201 plate of pre-cast resin of the same size as the box was placed on top of the clay. No
202 curing time is required, and the test can readily commence once the model is
203 assembled.
204 • 3D printed plastic-clay test: as for the pre-cast resin test, but a 3D printed plastic
205 plate is used.

206 4. Results

207 The main features of the centrifuge tests analysed in this paper are listed in Table 2, results
208 refer to the model scale. Some of the results (i.e. the ultimate capacity) from tests T12, T13
209 and T14 have been already presented in Lalicata *et al.* (2023), while the others belong to a
210 new set of centrifuge tests. From the whole set of data, only the pile load test results with
211 reliable and direct measurements of settlement are used. All the impression piles have four
212 nodules per cross section ($n = 4$) and values of vertical spacing lower than critical ($s < s_{cr}$).

213 4.1. Load settlement curves

214 The load-settlement curves for all the seventeen pile load tests are presented in Figure 9a
215 and b for the resin and plastic piles respectively. Settlement is represented in normalised
216 form.

Plastic piles, regardless of whether they are impression or plain piles, show a lower ultimate capacity indicating a lower value of the adhesion factor α, (see Table 2). Note that, α can be directly calculated from the plain pile tests only. For the impression pile, α is 1 along the vertical soil ribs connecting the nodules whilst elsewhere it is assumed equal to the value calculated from the plain pile in the same test, see Figure 2b. The load settlement response of the plain resin model piles is very different from that of the plastic model piles. Plain resin model piles show a marked peak at a settlement of 7-10% of the diameter, after which the load reduces to a stable ultimate value. The peak magnitude is highly variable being 1.15-1.52 times the value of the ultimate load. Whereas, the plastic model piles show a ductile behaviour, with a load that slowly increases after a significant reduction in gradient at w~5%d. These differences are related to the different interface behaviour of the two materials as manifest in the shear box results described below.

The impression model piles made from resin, exhibit a less marked peak than the corresponding plain model piles because a proportion of the failure surface is now in the soil and not at the soil pile interface. This proportion increases with an increase in active length.

The plastic model piles seem to have a better repeatability compared to the resin model piles. This is expected since the plastic is an industrial material with precise properties while the resin mixture is handmade for each model pile thus small differences in the preparation may influence the results, especially at low settlement levels. However, it should be noted that the larger number of pile tests available for the resin model piles and the natural experimental variability of the soil models, may be partly responsible for those differences.

The measured values of ultimate capacity, and the corresponding increase in capacity for the impression model piles are listed in Table 3 and Table 4 for resin and plastic model piles respectively. For the resin model piles, the capacity Q_u is defined as the asymptotic value of the curve after the peak where the shaft and the base resistance may be assumed fully

mobilised. The same method is not directly applicable to the plastic model piles as they show a hardening behaviour, see Figure 9b. For those piles, Q_u has been defined with different methods widely used in the literature: the settlement criterion (Kodsy *et al.*, 2022), the double tangent and the hyperbolic method defined by Chin (Chin, 1970).

The settlement criterion assumes the pile capacity is attained at a given value of displacement, typically equal to 10%*d*, regardless of the actual shape of the load-settlement curve. Here, *w*=25%*d* is also used because, as suggested by Mandolini *et al.* (2005), bored piles may need larger settlement values to fully mobilise their capacity. The double tangent method defines the ultimate capacity as the intersection between the tangent at *w/d*=0 (initial stiffness) and the tangent to the load-settlement curve at large displacements. It is worth noting that with this method the ultimate capacity is attained at very small settlements (w~1 – 1.2%*d*). The Chin method interpolates the experimental curve with a hyperbolic function, whose parameters are the initial stiffness and the capacity Q_u. As suggested by many authors, the capacity is set equal to 90% of the capacity obtained from the best fit parameters derived from the Chin interpolation.

Irrespective of the method used to define the ultimate capacity, the plastic model piles show, in general, a higher increase in ultimate capacity (~40%) compared to the resin model piles (~20%) with similar L_a values (0.75 and 0.78 respectively). This result is consistent with the smaller values of adhesion factor measured for the plastic model piles, as decreasing the value of α, increases the importance of the soil-soil shearing created by the nodules.

The increase in capacity of the plastic impression model piles reduces for increasing *w/d* values because the progressive mobilisation of the base resistance acts at both the numerator and the denominator. The increase in ultimate capacity is highest when calculated using the double tangent method, but the scatter in these values is also highest, varying from 46 to 68%. Consistent increases in capacity of around 37% are obtained using

the Chin interpolation or a settlement criterion of w=25%d and they appear to provide the best representation of the full mobilisation of the capacity of the model pile.

4.2. Small strain behaviour

To examine the performance of the model pile at small displacements, secant stiffness is plotted against normalised settlement in a semi-log plane in Figure 10.

The range of interest (w/d=0.3% - 2%) is highlighted in the figure. Measurements of displacement below w/d=0.3%, w=0.048mm, cannot be determined accurately, as the sum of the accuracy of the micrometre used for the calibration, ±0.01mm, and that of the LVDTs itself, ±0.02mm, gives an overall accuracy of ±0.03mm which is 60% of the displacement at w/d=0.3%. Above w/d=2% the piles are at 45-88% of ultimate capacity and consequently not all the piles could be considered to be under working load conditions.

Data from tests on resin model piles, Figure 10a, are highly scattered at w/d<1% making it difficult to discern a clear difference between the response of the plain or impression model piles. It appears that the high interface strength of the resin, before the peak capacity is reached, obscures the effect of the nodules on working load behaviour.

Conversely, the effect of the impressions on the working load behaviour of the plastic model piles is clear, Figure 10b. In this case, the impression model piles show a significant increase in secant stiffness at every load level, for instance, equal to ~90% and ~73% at w/d=0.3% and 0.5%, respectively. For increased clarity, the ratio between the load taken by the impression pile and the load taken by the plain pile at the corresponding displacement in each test is shown in Figure 11. The coloured areas represent the experimental range of the data. Plastic model piles show a smooth decrease in load ratio with settlement from 1.9 at w/d=0.3% to 1.4 at capacity (w/d=25% in the plot). Whereas resin model piles show a large variability at small displacements, the load ratio ranging from 0.6 to 1.2, i.e. lower than unity

in some cases. After *w/d*=10%, there is an increase in the load ratio because the plain piles have reached ultimate capacity and the increase in capacity ranges between 1.2 and 1.5 as already discussed in the previous section.

The average values of the secant stiffness at selected settlement levels are listed in Table 5. To allow a direct comparison between the resin and plastic impression model piles, only similar piles are included in this table (i.e. all the impression model piles with $L_a/L \sim 0.75$, see Table 2). The lower scatter in the data measured for the plastic model piles confirms the greater consistency of the plastic-soil interface and the lower variability of the 3D printed plastic compared to the cast in place resin. From both Table 5 and Figure 10 it is clear that the resin model piles have a stiffer response compared to plastic model piles at any displacement level.

The last two columns in Table 5 list the secant stiffness ratio (equivalent to the load ratio) for the resin and plastic model piles for the plain and the impression model piles respectively. This ratio increases for increasing values of *w/d,* and it is larger for the plain pile case, for any *w/d* value. The plain pile resin to plastic ratio is representative of the material properties only. It is interesting to note that, even at very small displacement values (*w/d*=0.5%), this ratio is larger than the stiffness ratio of the two materials ($E_{resin}/E_{plastic}$=1.1GPa/0.75GPa=1.46). The rationale can be found in the different shape of the load-settlement curves (see Figure 9) that is linked to the shear stress mobilisation along the shaft. For the impression model piles the ratio is lower (it ranges from 1.14 to 1.85) because the presence of the nodules creates a slip plane away from the shaft and, consequently, the differences in the interface behaviour are masked even at small strains.

4.3. Direct shear tests

The results of the direct shear tests are depicted in Figure 12, where the shear stress has been normalised by the undrained shear strength, evaluated from water content

316 measurements via eq. (1). The tests using clay only with no interface are fairly consistent,
317 with a peak that is approximately equal to $0.9s_u$. The results from tests where there was an
318 interface with precast resin and plastic show τ/s_u values that become constant after a small
319 peak at displacements of between 0.5 and 1.5mm, indicating that failure has occurred. The
320 ultimate τ/s_u values are ~0.50 and ~0.33 for the precast resin and the plastic respectively,
321 Table 6.

322 In contrast, the cast resin test results are significantly steeper at the beginning than the other
323 curves and reach a large peak stress (of 2 and 3.25 times s_u); in the softening that follows,
324 τ/s_u reduces to ~0.57 that is close to the value measured in the precast resin tests.
325 Although the two tests carried out on the cast in place resin look very different, it should be
326 noted that they share the same value of τ/s_u at large displacements.

327 It is thought that the reason for this behaviour is the curing process of the resin against the
328 clay. The curing phase is an exothermic chemical process (McNamara & Taylor, 2009), thus
329 a thin clay layer around the pile is likely to experience some heating and possibly some
330 chemical bonding with the resin, affecting the properties of the soil-resin interface. In the
331 direct shear tests, the peak is significantly larger than would be consistent with the pile
332 response observed in the centrifuge tests (see Figure 9a) because, in the latter, pore
333 pressures are allowed to come into equilibrium at 50*g* for 48 hours and this will mitigate most
334 of the effects the exothermic reaction has on water contents near the pile. Conversely, in the
335 shear box tests, the samples were sheared just after the end of the curing process.

336 5. Discussion

337 Previous research on ribbed and impression model piles (Figure 1 and Figure 9a) seemed to
338 suggest that those model piles needed to experience a relatively large head settlement
339 before being able to mobilise the enhanced shaft resistance provided by the profiling of the

model pile shaft. However, the results presented have indicated that this conclusion was a function of the material used to cast the model pile. Changing the material, but not the geometry of the impression model piles, a different behaviour has been observed (Figure 11). These new data suggest that in the tests on cast *in situ* resin model piles, the effect of the nodules on the working load behaviour of the impression resin model pile is masked by the properties of the soil-resin interface. All the resin plain model piles show a peak and a softening. Often, the peak load achieved by the plain model piles is close to the capacity of the impression model piles in the same test. A similar strain-softening behaviour observed in the plain resin model piles has been found in model tests on epoxy resin (Araldite) piles (Chandler and Martins, 1982) but is seldom observed in full scale tests on traditional bored concrete piles, probably because other technological factors play a major role in this case and the curing process will be different between the resin and the concrete.

However, with a printed plastic model pile, the soil-plastic interface is stable and relatively smooth. This means that the maximum allowable shear stress on the interface will be always lower than that of the soil and consequently, when the failure surface is moved away from the pile due to the presence of the nodules the shaft resistance of the model pile will necessarily increase, resulting in a soil-pile secant stiffness (or load) which is always higher for the impression model pile at a given displacement.

On site, there is limited evidence of the concrete curing effects on the skin friction of piles (Mascarucci & Mandolini, 2013) and a detailed study of the curing effect of the resin is outside the scope of this study. However, the direct shear tests carried out confirm the centrifuge test findings. The peak-softening behaviour of the resin only occurs when the resin is cast against the soil affecting the soil close to the shaft interface. When the resin is not cast *in situ* the peak resistance reduces to values close to the ultimate resistance in line with the observations of other authors (Yavari *et al.*, 2016; Parchment & Shepley, 2018). The ultimate resistance of the “cast in place” resin is similar to that of the “precast” resin,

suggesting that particle rearrangement at the interface upon shearing finally overcomes the curing effects.

Conclusions

A novel experimental technique to model impression piles has been presented in this paper. The novel model piles (both impression and plain) are made of 3D printed rigid plastic components assembled during the installation process.

The behaviour of these plastic model piles has been investigated by means of geotechnical centrifuge testing on overconsolidated clay samples. In each test, the impression model piles were tested together with one plain model pile against which the impression model piles could be assessed. Installation effects are neglected as the model piles were installed at 1*g* rather than in the high-*g* environment. This is clearly not representative of the prototype scale installation, but may be considered as an ideal wished-in-place installation of the pile. Results from five model pile load tests have been compared with resin model piles of similar geometry and tested in similar conditions. The tests on the plastic model piles showed an excellent repeatability across the two centrifuge tests on both the two plain model piles and the three impression model piles.

The method of installation of the plastic model piles reduced experimental variability and eliminated the consequences of the curing process on the cast resin model piles. This helped to highlight the beneficial effects of the impressions on the whole load-settlement curve, from small strain to capacity.

Plastic plain model piles showed a monotonically increasing load settlement curve while resin plain model piles had a marked strain softening behaviour. Consequently, the impression plastic model piles outperformed the plain plastic model piles at any pile displacement. These results suggest that the displacement needed to mobilise the enhanced

shaft capacity of the impression piles is small and of the same order of magnitude of that needed to mobilise the skin friction in ordinary bored piles, making the impression pile solution attractive. Such behaviour was not observed in the resin model piles due to the high shear resistance of the interface induced by the curing process of the resin. In those model piles, the improved performance of the impression model piles was clear only at ultimate capacity. Qualitatively, the significance of the type of pile-soil interface has been confirmed by rapid direct shear interface tests, which demonstrated that the curing process of the resin significantly affected the peak resistance of the interface. At large displacements, the particle rearrangement at the interface during shearing finally overcomes the curing effects and the ultimate resistance of the cast *in situ* resin is similar to the precast resin.

To date, the set of data available is not sufficient to quantify the impact of different impression geometries on the working load behaviour of the impression piles, but further tests are planned to enlarge the experimental dataset.

Acknowledgements

This research project would not have been developed without funding from Innovate UK and the vision of Keltbray Piling. They are gratefully acknowledged. The authors also want to thank Mr Keith Pamment from City, University of London for his support in the development of the 3D printed impression pile.

CRediT authorship contribution statement

Leonardo Maria Lalicata: Conceptualisation, Methodology, Validation, Formal analysis, Investigation, Data curation, Writing – original draft, Visualisation, Project administration. **Eric Ritchie**: Investigation. **Sarah Elizabeth Stallebrass**: Conceptualisation, Methodology, Writing – Review & Editing, Supervision, Project administration, Funding acquisition. **Andrew McNamara**: Conceptualisation, Methodology, Writing – Review & Editing, Supervision, Project administration, Funding acquisition.

References

Al-Defae, A. H., & Knappett, J. A. (2014). Centrifuge modeling of the seismic performance of pile-reinforced slopes. *Journal of Geotechnical and Geoenvironmental Engineering*, *140*(6), 04014014.

Alnuaim, A. M., El Naggar, M. H., & El Naggar, H. (2015). Performance of micropiled raft in clay subjected to vertical concentrated load: Centrifuge modelling. *Canadian Geotechnical Journal*, *52*(12), 2017–2029. https://doi.org/10.1139/cgj-2014-0448

Chandler, R. J., & Martins, J. P. (1982). An experimental study of skin friction around piles in clay. *Géotechnique*, *32*(2), 119–132. https://doi.org/10.1680/geot.1982.32.2.119

Chin, F.V. (1970). Estimation of the ultimate load of piles not carried to failure. *Proceedings of the 2nd Southeast Asian Conference on Soil Engineering*, Singapore, pp. 81–90.

de Sanctis, L., Di Laora, R., Garala, T. K., Madabhushi, S. P. G., Viggiani, G. M. B., & Fargnoli, P. (2021). Centrifuge modelling of the behaviour of pile groups under vertical eccentric load. *Soils and Foundations*, *61*(2), 465–479. https://doi.org/10.1016/j.sandf.2021.01.006

Divall, S., & Goodey, R. J. (2015). Twin-tunnelling-induced ground movements in clay. *Proceedings of the Institution of Civil Engineers - Geotechnical Engineering*, *168*(3), 247–256. https://doi.org/10.1680/geng.14.00054

Goode, J. C. III, & McCartney, J. S. (2015). Centrifuge modeling of end-restraint effects in energy foundations. *J. Geotech. Geoenviron. Eng*, *141*(8), https://doi.org/10.1061/(ASCE)GT.1943-5606.0001333

Gorasia, R. J., & McNamara, A. (2016). High-capacity ribbed pile foundations. *Proceedings of the Institution of Civil Engineers - Geotechnical Engineering*, *169*(3), 264–275. https://doi.org/10.1680/jgeen.15.00073

Hard, D. A. & Carvalho, A. T. (2018). Threaded rotary bored piles at Paddington new yard. Proceedings of the 2018 *DFI-EFFC international conference on deep foundations and ground improvement*, Rome, Italy.

Iovino, M., Iodice, C., Alagha, A., & Viggiani, G. M. (2023). Centrifuge Experiments Dealing with Monotonic and Cyclic Loads on Pile Foundations in Sand. In: Ferrari, A., Rosone, M., Ziccarelli, M., Gottardi, G. (eds) *Geotechnical Engineering in the Digital and Technological Innovation Era. CNRIG 2023*. Springer Series in Geomechanics and Geoengineering. Springer, Cham. https://doi.org/10.1007/978-3-031-34761-0_81

Knappett, J. A., Reid, C., Kinmond, S., & O'Reilly, K. (2011). Small-scale modeling of reinforced concrete structural elements for use in a geotechnical centrifuge. *Journal of Structural Engineering*, *137*(11), 1263-1271.

Kodsy, A., Iskander, M. G., & Sampurnanand Pandey, A. (2022). Universal Criterion for Interpreting Capacity from Load Tests on Piles. *Transportation Research Record: Journal of the Transportation Research Board*, 036119812210846. https://doi.org/10.1177/03611981221084686

Lalicata, L. M., Desideri, A., Casini, F., & Thorel, L. (2019). Experimental observation on laterally loaded pile in unsaturated silty soil. *Canadian Geotechnical Journal*, *56*(11), 1545–1556. https://doi.org/10.1139/cgj-2018-0322

Lalicata, L. M., McNamara, A. M. & Stallebrass, S. E. (2020a). Experimental technique for creating enhanced capacity piles in a centrifuge environment. *In Proceedings of the*

European conference on physical modelling in geotechnics ECPMG2020, pp. 49–55. Luleå, Sweden: Luleå University of Technology.

Lalicata, L. M., Rotisciani, G. M., Desideri, A., Casini, F., & Thorel, L. (2020b). Physical modelling of piles under lateral loading in unsaturated soils. *In 4th European Conference on Unsaturated Soils, E-UNSAT 2020.* Cardoso R., Jommi C., Romero E. (Eds). E3S Web of Conferences 195(01021). https://doi.org/10.1051/e3sconf/202019501021

Lalicata, L. M., Stallebrass, S. E., & McNamara, A. (2023). An experimental study into the ultimate capacity of an 'impression' pile in clay. *Géotechnique*, 73(5), 455-466. https://doi.org/10.1680/jgeot.21.00168

Lalicata, L. M., Stallebrass, S. E., McNamara, A., & Panchal, J. P. (2022). Design method for the 'impression pile'. *Proceedings of the Institution of Civil Engineers - Geotechnical Engineering*, *175*(1), 75–85. https://doi.org/10.1680/jgeen.21.00033

Le, B. T., & Taylor, R. N. (2018). Response of clay soil to three-dimensional tunnelling simulation in centrifuge models. *Soils and Foundations*, *58*(4), 808–818. https://doi.org/10.1016/j.sandf.2018.03.008

Li, Q., Askarinejad, A., & Gavin, K. (2022). Lateral response of rigid monopiles subjected to cyclic loading: Centrifuge modelling. *Proceedings of the Institution of Civil Engineers - Geotechnical Engineering*, *175*(4), 426-438. https://doi.org/10.1680/jgeen.20.00088

Li, Z.-S., Blanc, M., & Thorel, L. (2023). Effects of embedding depth and load eccentricity on lateral response of offshore monopiles in dense sand: A centrifuge study. *Géotechnique*, *73*(9), 811-825. https://doi.org/10.1680/jgeot.21.00200

Maatouk, S., Blanc, M., & Thorel, L. (2022). Impact driving of monopiles in centrifuge: Effect on the lateral response in sand. *International Journal of Physical Modelling in Geotechnics*, *22*(6), 318-331. https://doi.org/10.1680/jphmg.21.00035

Mandolini, A., Russo, G. & Viggiani, C. (2005). Piled foundations: experimental investigations, analysis and design, State-of-the-art report. *In Proceedings of the 16th international conference on soil mechanics and geotechnical engineering: geotechnology in harmony with the global environment*, vol. 1, pp. 177–213. Rotterdam, the Netherlands: Millpress.

Mascarucci, Y., Mandolini, A., & Miliziano, S. (2013). Effects of residual stresses on shaft friction of bored cast in situ piles in sand. *Journal of Geo-Engineering Sciences*, *1*(1), 37–51. https://doi.org/10.3233/JGS-13009

McNamara, A. M. & Taylor, R. N. (2002). Use of heave reducing piles to control ground movements around excavations. *In Physical modelling in geotechnics: proceedings of international conference ICPGM'02* (eds P. Guo, R. Phillips and R. Popescu), pp. 847–852. Rotterdam, the Netherlands: Balkema.

McNamara, A. M. (2001). Influence of heave reducing piles on ground movements around excavations. PhD thesis, City University, London, UK.

McNamara, A. M., Goodey, R. J. & Taylor, R. N. (2009). Apparatus for centrifuge modelling of top down basement construction with heave reducing piles. *Int. J. Phys. Modelling Geotech*, 9(1), 1–14, https:// https://doi.org/10.1680/ijpmg.2009.9.1.01.

Ng, C. W. W., Shi, C., Gunawan, A., & Laloui, L. (2014). Centrifuge modelling of energy piles subjected to heating and cooling cycles in clay. *Géotechnique Letters*, *4*(4), 310–316. https://doi.org/10.1680/geolett.14.00063

Ouzzine, B., de Sauvage, J., Madabhushi, G., Viggiani, G., & Reiffsteck, P. (2023). Centrifuge modelling of an energy pile group with ground water flow. *International*

Journal of Physical Modelling in Geotechnics, 1-25. https://doi.org/10.1680/jphmg.22.00041

Parchment, J., & Shepley, P. (2018). The influence of temperature on shear strength at a soil-structure interface. In A. McNamara, S. Divall, R. Goodey, N. Taylor, S. Stallebrass, & J. Panchal (Eds.), *Physical Modelling in Geotechnics* (1st ed., pp. 149–154). CRC Press. https://doi.org/10.1201/9780429438660-15

Phillips, R. (1995). Centrifuge modelling: practical considerations. *In Geotechnical centrifuge technology* (ed. R. N. Taylor), Ch. 3, pp. 34–59. Glasgow, UK: Blackie Academic and Professional. https://doi.org/10.1201/9781482269321-3

Rollins, K. M., Lane, J. D., & Gerber, T. M. (2005). Measured and Computed Lateral Response of a Pile Group in Sand. *Journal of Geotechnical and Geoenvironmental Engineering*, *131*(1), 103–114. https://doi.org/10.1061/(ASCE)1090-0241(2005)131:1(103)

Rosquoët, F., Thorel, L., Garnier, J., & Canepa, Y. (2007). Lateral Cyclic Loading of Sand-Installed Piles. *Soils and Foundations*, *47*(5), 821–832. https://doi.org/10.3208/sandf.47.821

Schofield, A. N. & Taylor, R. N. (1988). Development of standard geotechnical centrifuge operations. *In Centrifuge 88: proceedings of the international conference on geotechnical centrifuge modelling* (ed. J.-F. Corté), pp. 29–32. Rotterdam, the Netherlands: Millpress.

Shabanpour, A., & Ghazavi, M. (2022). Centrifuge tests on axially loaded tapered piles with different cross-sections under compressive and tensile loading. *Canadian Geotechnical Journal*, *59*(7): 1205-1214. https://doi.org/10.1139/cgj-2020-0732

Taylor, R. N., Rose, A. V., & Gorasia, R. J. (2013). Pile and Pile Group Capacity: Some Findings from Centrifuge Tests. *Int. J. Geotech. Engng 5*(2), 5-15.

Truong, P., Lehane, B. M., Zania, V., & Klinkvort, R. T. (2019). Empirical approach based on centrifuge testing for cyclic deformations of laterally loaded piles in sand. *Géotechnique*, *69*(2), 133–145. https://doi.org/10.1680/jgeot.17.P.203

Wood, D. M. (2004). *Geotechnical modelling*. New York, NY, USA: Spon Press.

Yavari, N., Tang, A. M., Pereira, J. M., & Hassen, G. (2016). Effect of temperature on the shear strength of soils and the soil–structure interface. *Canadian Geotechnical Journal*, *53*(7), 1186-1194. https://doi.org/10.1139/cgj-2015-0355

Zhao, R., Leung, A. K., Vitali, D., Knappett, J. A., & Zhou, Z. (2020). Small-scale modeling of thermomechanical behavior of reinforced concrete energy piles in soil. Journal of Geotechnical and Geoenvironmental Engineering, 146(4), 04020011. https://doi.org/10.1061/(ASCE)GT.1943-5606.0002225

List of Figures

List of Tables

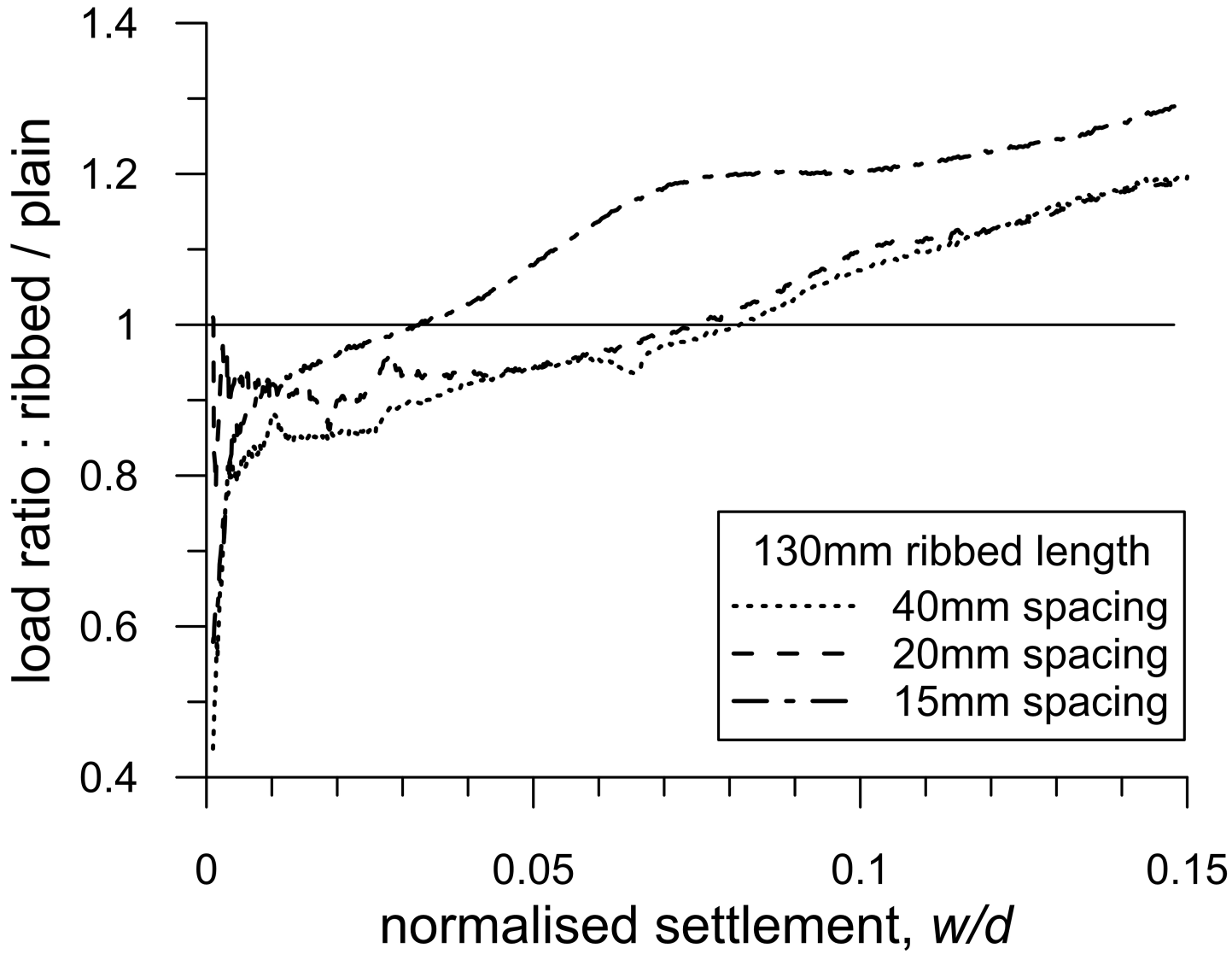
1.4
1.2
1
0.8
0.6
0.4
load ratio : ribbed / plain
0
0.05
0.1
0.15
normalised settlement, w/d
130mm ribbed length
40mm spacing
20mm spacing
15mm spacing

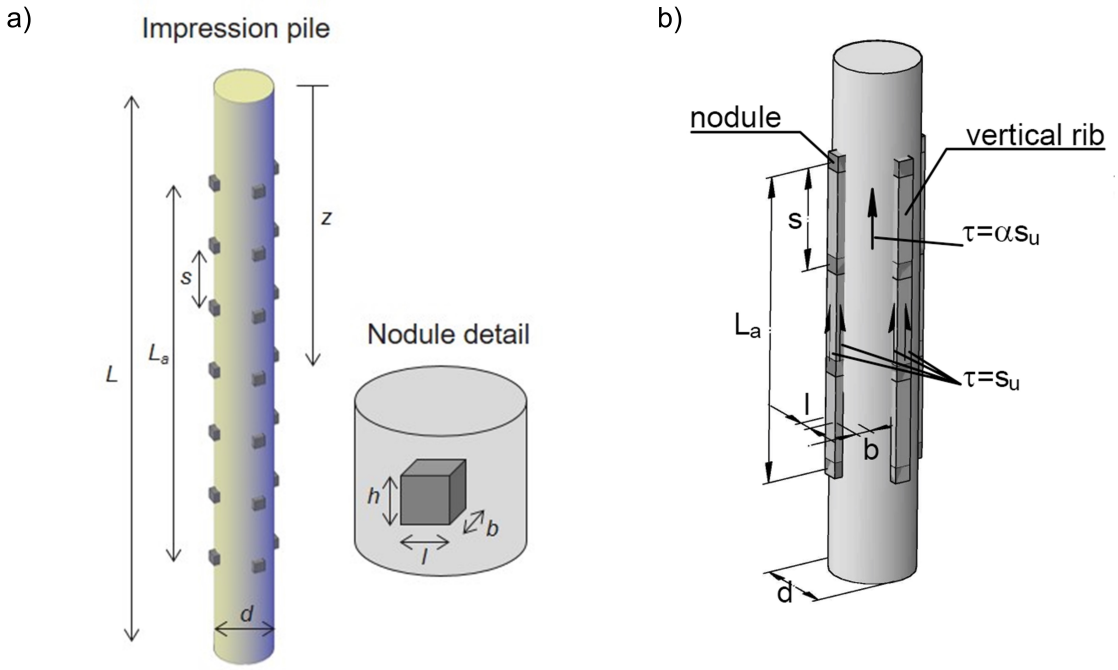
a)
Impression pile
z
s
L
L_a
d
Nodule detail
h
b
l
b)
nodule
vertical rib
s
$\tau=\alpha s_u$
L_a
$\tau=s_u$
l
b
d

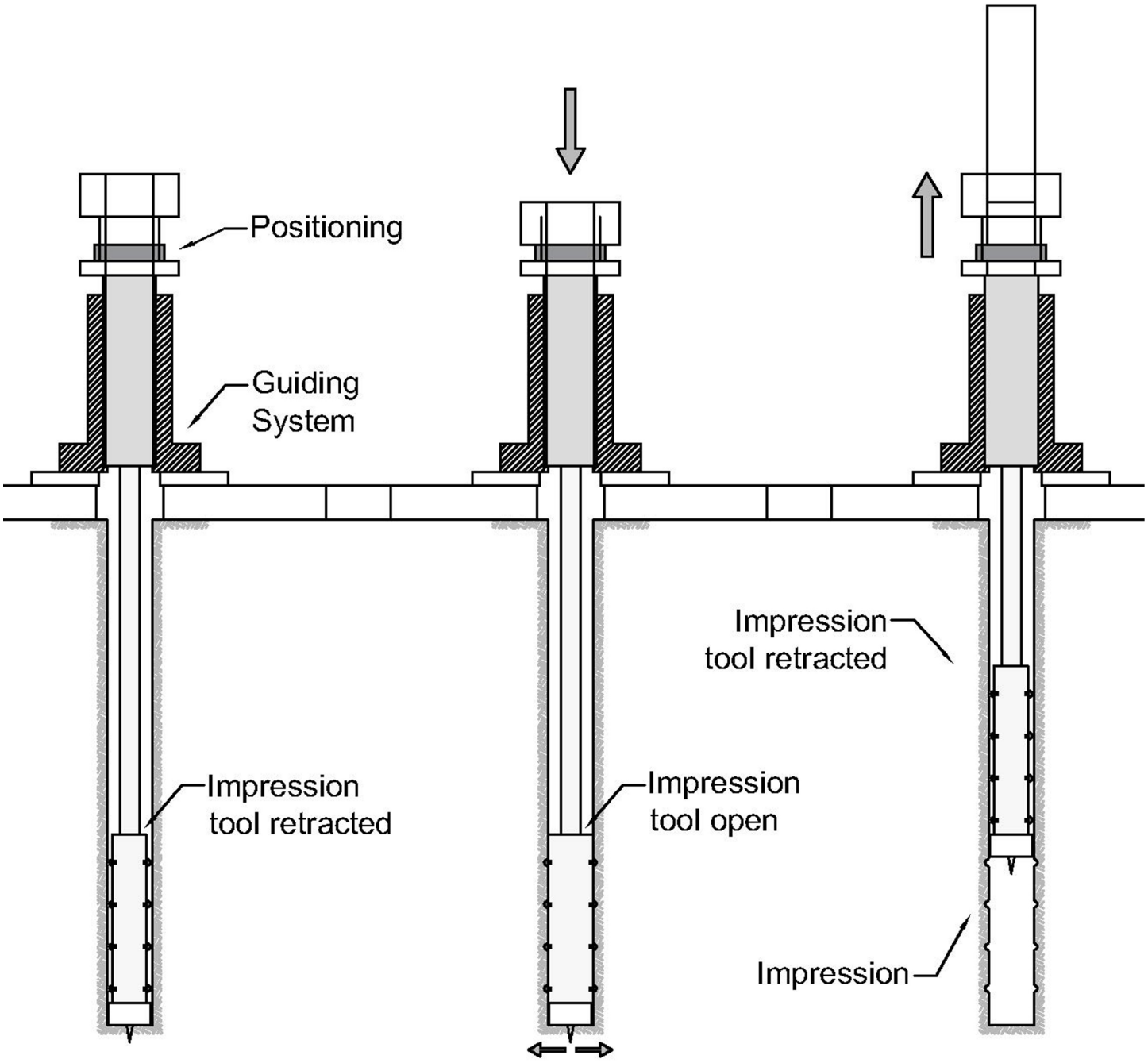
Positioning
Guiding System
Impression tool retracted
Impression tool retracted
Impression tool open
Impression

a) Resin Piles

b) 3D Printed Piles

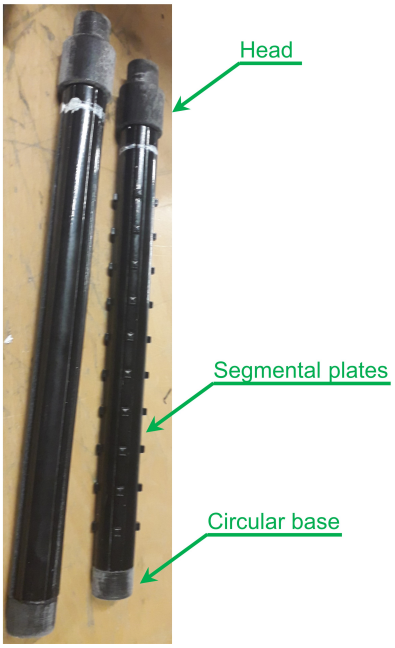

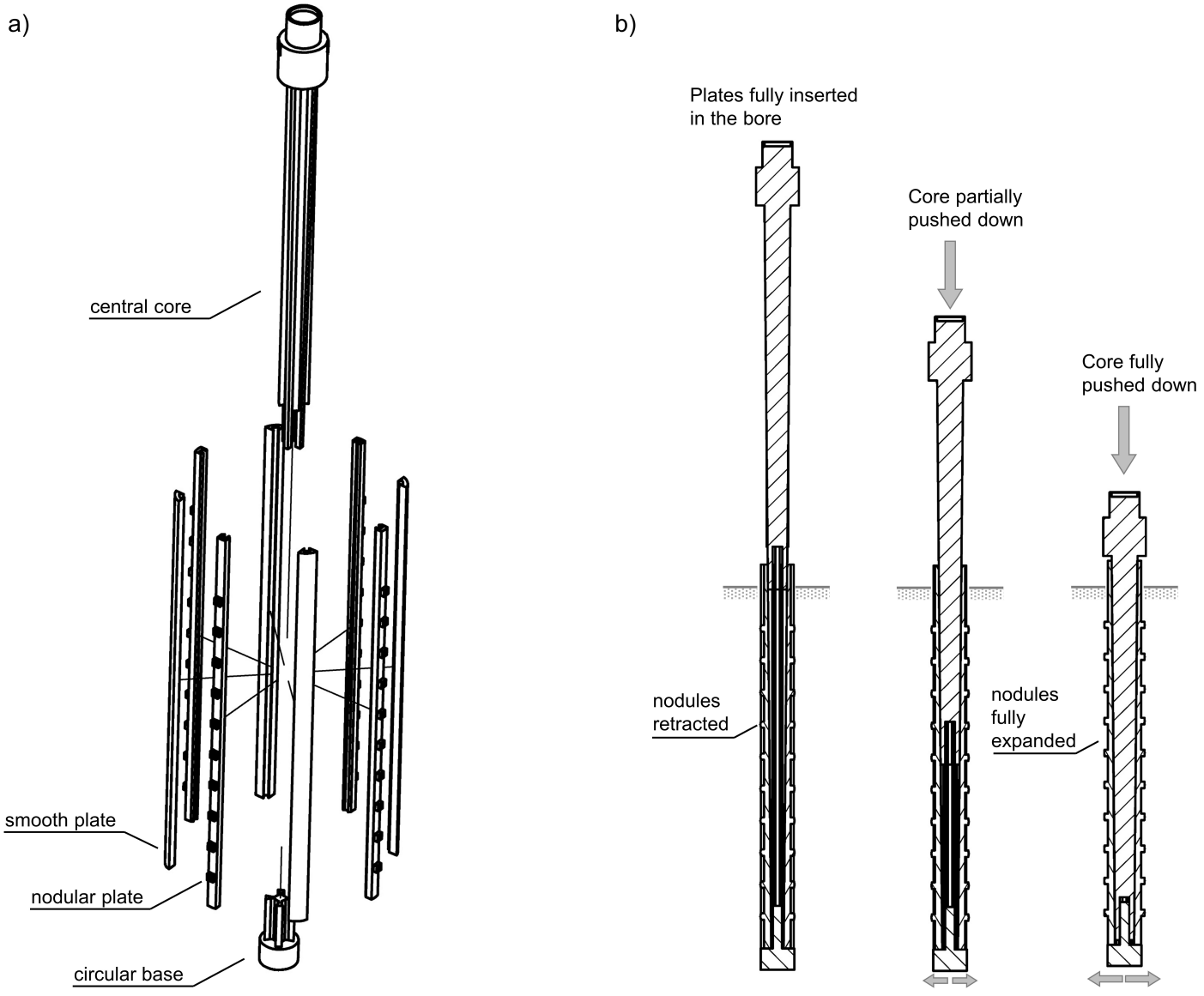
a)
central core
smooth plate
nodular plate
circular base
b)
Plates fully inserted
in the bore
Core partially
pushed down
Core fully
pushed down
nodules
retracted
nodules
fully
expanded


Central core
Fully retracted nodular plates
Smooth plates
Concave plate
LVDTs' plate

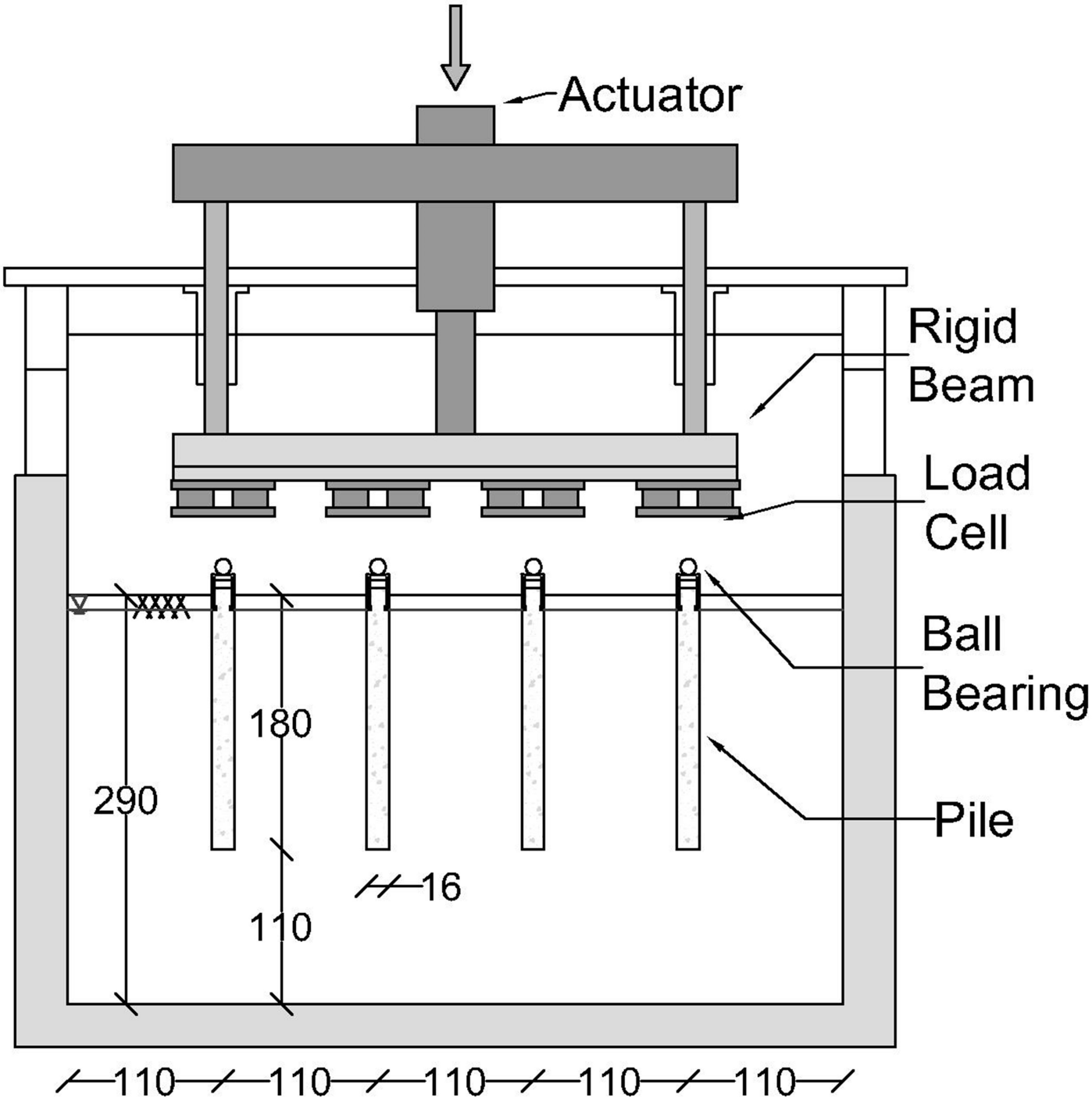
Actuator
Rigid
Beam
Load
Cell
Ball
Bearing
Pile
180
290
16
110
110
110
110
110
110

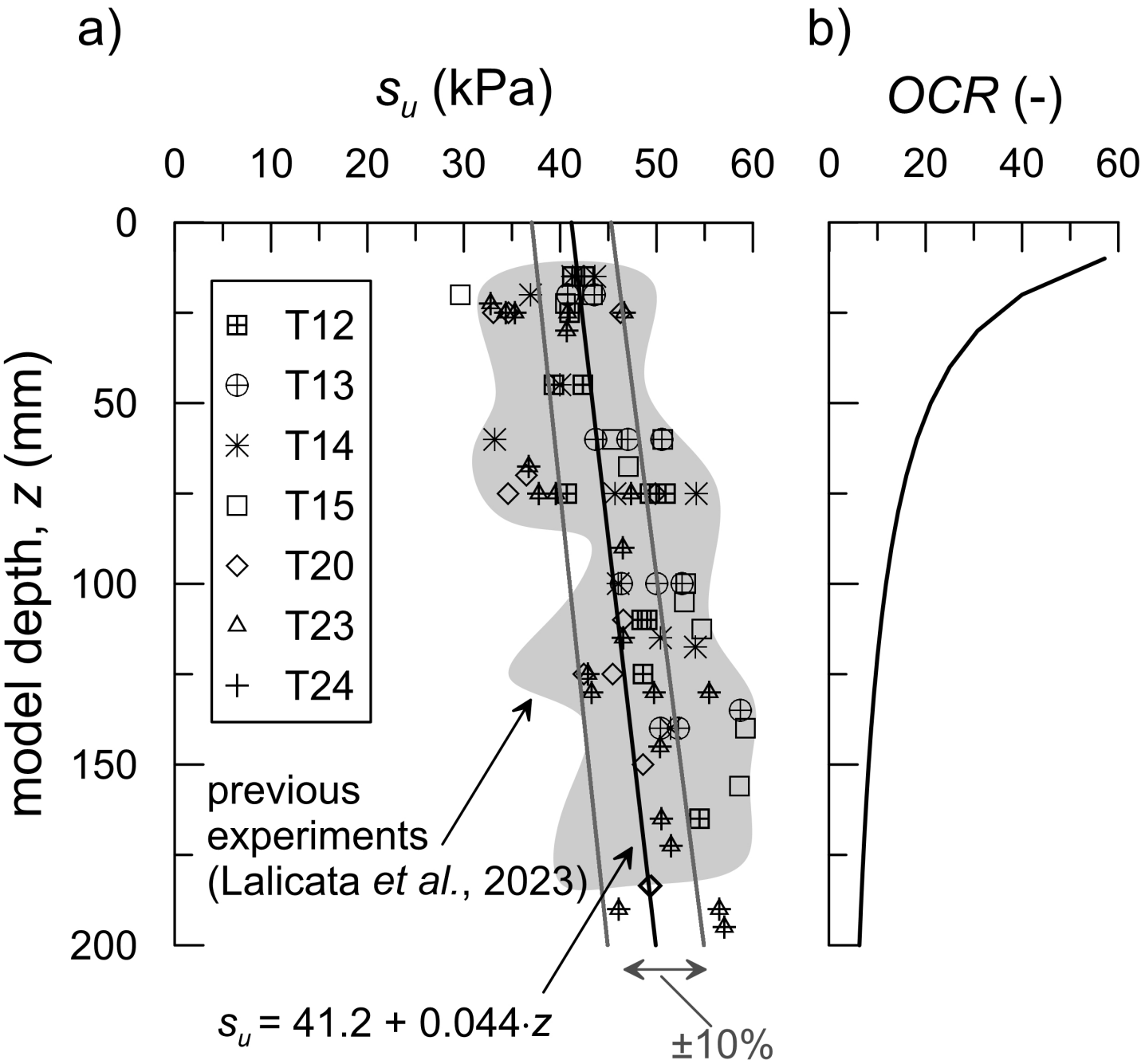
a)
b)
s_u (kPa)
OCR (-)
0 10 20 30 40 50 60
0 20 40 60
model depth, z (mm)
0
50
100
150
200
T12
T13
T14
T15
T20
T23
T24
previous experiments (Lalicata et al., 2023)
s_u = 41.2 + 0.044·z
±10%

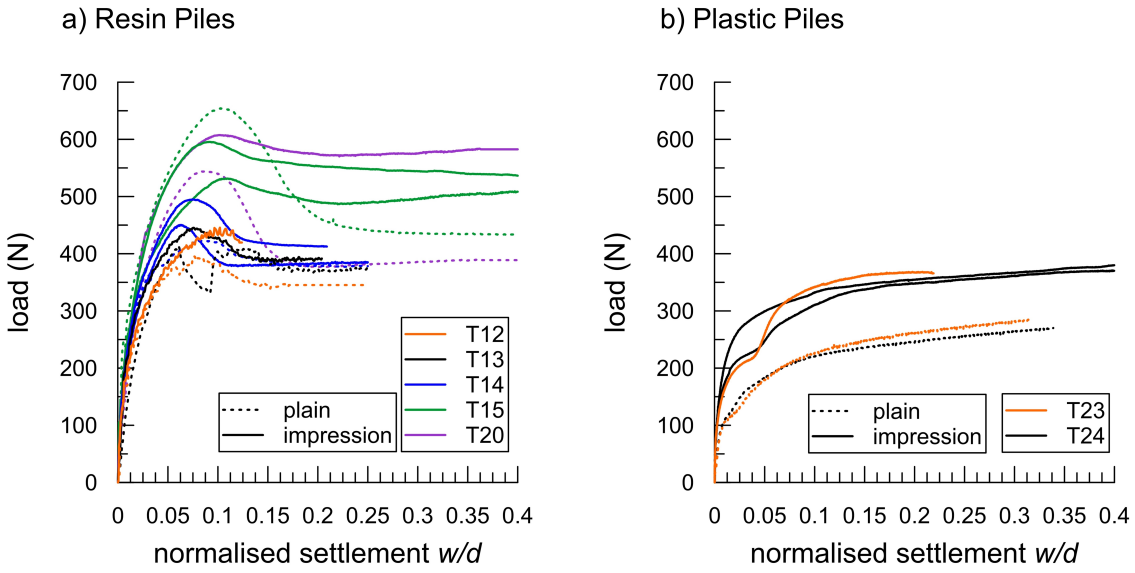
a) Resin Piles
b) Plastic Piles
load (N)
normalised settlement w/d
0
100
200
300
400
500
600
700
0 0.05 0.1 0.15 0.2 0.25 0.3 0.35 0.4
plain
impression
T12
T13
T14
T15
T20
T23
T24

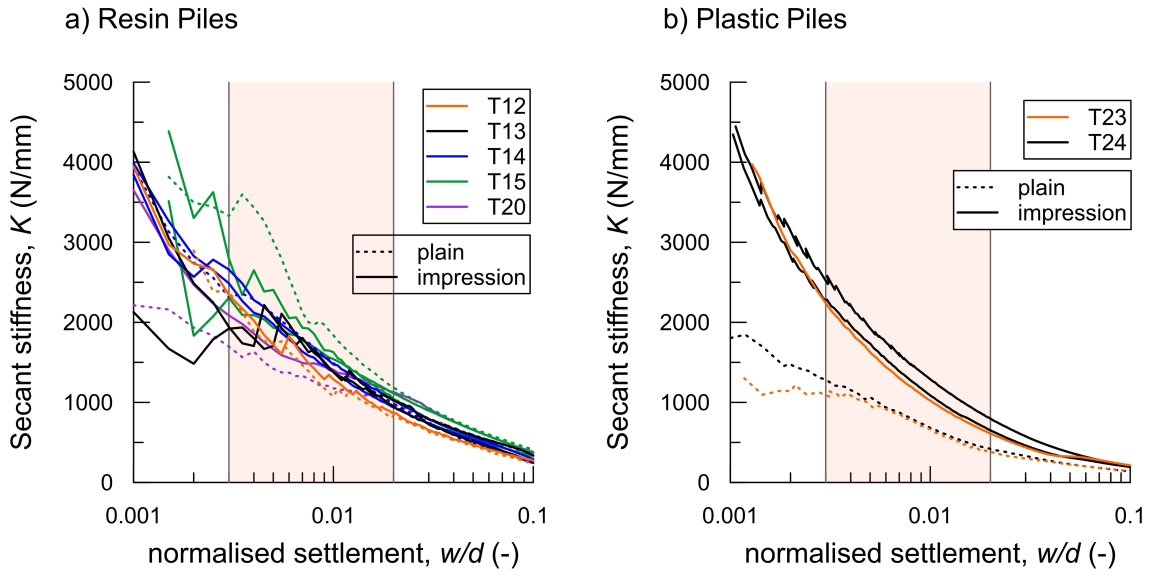
a) Resin Piles
b) Plastic Piles
Secant stiffness, K (N/mm)
normalised settlement, w/d (-)
5000
4000
3000
2000
1000
0
0.001
0.01
0.1
T12
T13
T14
T15
T20
T23
T24
plain
impression

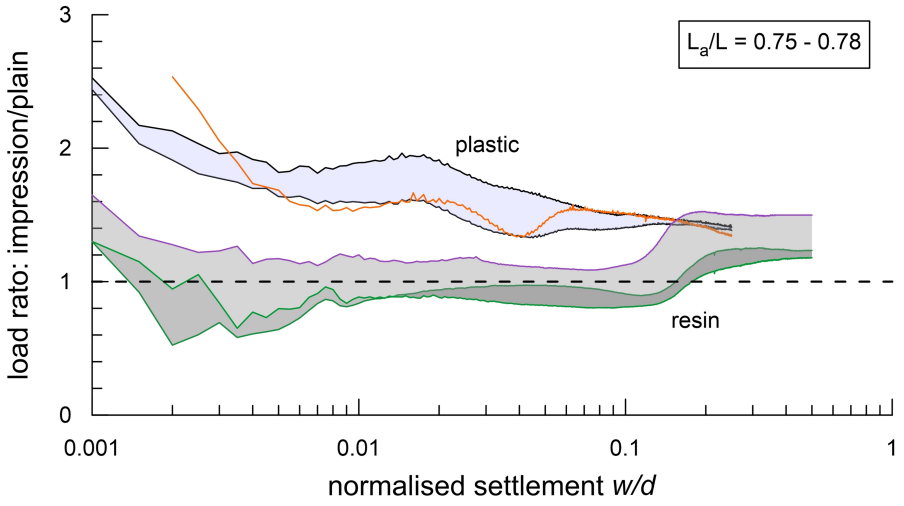
3
2
1
0
load rato: impression/plain
L_a/L = 0.75 - 0.78
plastic
resin
0.001
0.01
0.1
1
normalised settlement *w/d*

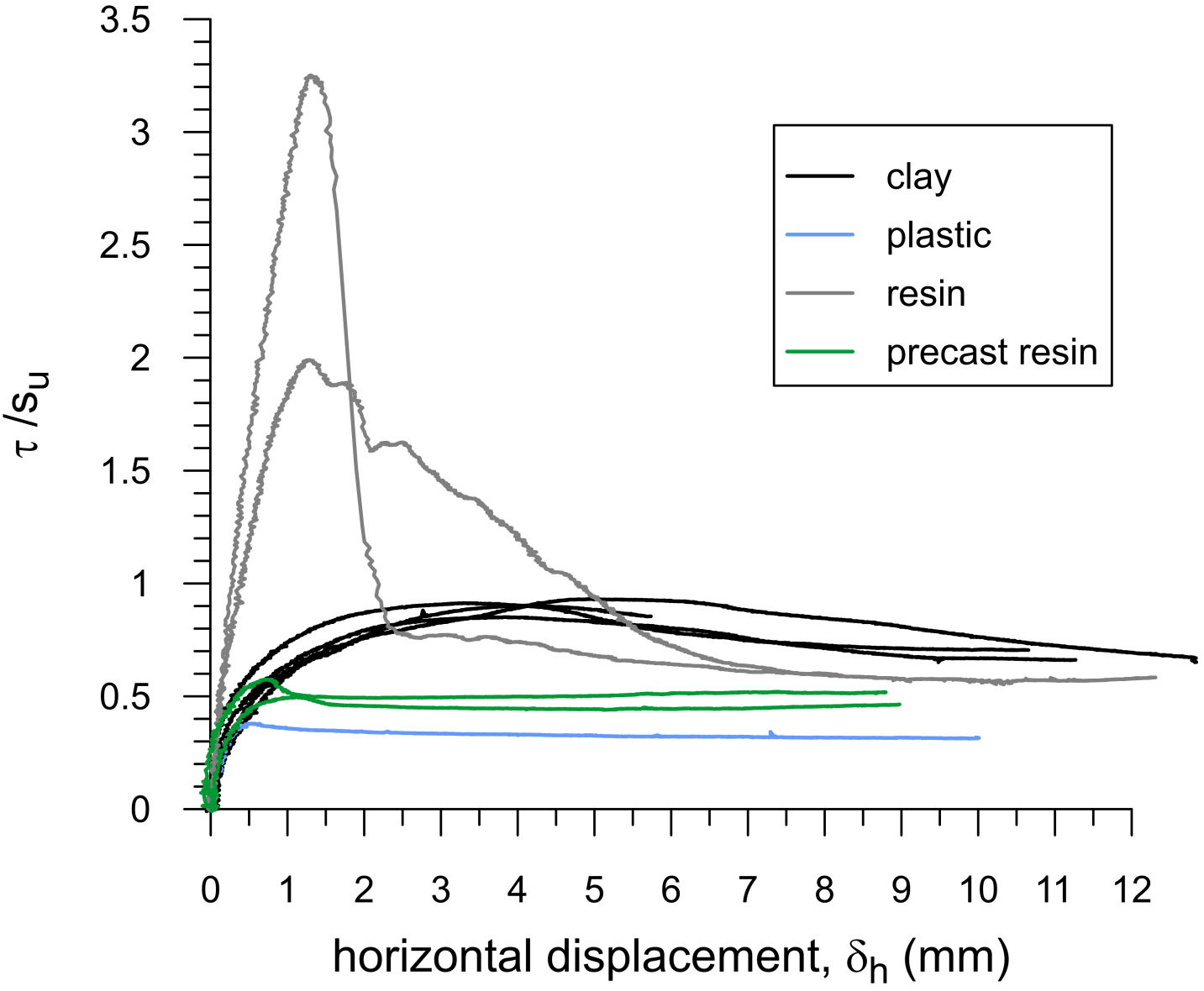
3.5
3
2.5
2
1.5
1
0.5
0
τ /su
0 1 2 3 4 5 6 7 8 9 10 11 12
horizontal displacement, δh (mm)
clay
plastic
resin
precast resin

Table 1. Mechanical parameters of the Speswhite Kaolin clay.

Parameter	Value
Slope of the critical state line in the q-p' space, *M*	0.89
Specific volume on the critical state line at p'=1kPa, Γ	3.04
Slope of the normal compression line in the *v-lnp'* space, λ	0.18
Specific gravity, G_s	2.61
Unit weight of soil, γ (kN/m^3)	17.5
Coefficient of vertical consolidation, c_v (mm^2/s)	0.45

Table 2. Summary of the centrifuge tests.

Test ID	Material	Pile Type	Normalised Active Length, La/L	Dead Weight, W (N)	Adhesion factor, α
T12	resin	plain		46	0.66
		impression	0.67	46	
T13	resin	plain		46	0.74
		impression	0.29	46	
T14	resin	plain		46	0.74
		impression	0.29	46	
		impression	0.29	46	
T15	resin	plain		46	0.88
		impression	0.78	46	
		impression	0.78	46	
T20	resin	plain		46	0.77
		impression	0.78	46	
T23	plastic	plain		43	0.47
		impression	0.75	43	
T24	plastic	plain		43	0.41
		impression	0.75	43	
		impression	0.75	43	

Table 3: Capacity and increase in capacity of the resin piles.

Resin	La/L	Graphical method	
		capacity, Qu (N)	Increase in capacity (-)
plain_T12	-	342	-
plain_T13	-	375	-
plain_T14	-	375	-
plain_T15	-	432	-
plain_T20	-	389	-
impression_T13	0.29	390	*1.04*
impression_T14	0.29	410	*1.09*
impression_T14	0.29	390	*1.04*
impression_T15	0.78	531	*1.23*
impression_T15	0.78	510	*1.18*
impression_T20	0.78	583	*1.5*

Table 4: Capacity and increase in capacity of the plastic piles.

		Methods to estimate the pile's capacity							
		settlement				Double tangent		Chin	
		w/d = 10%		w/d = 25%		w/d ~ 1 – 1.2%		0.9*Chin	
Plastic Pile	L_a/L	capacity, Q_u (N)	Increase in capacity (-)	capacity, Q_u (N)	Increase in capacity (-)	capacity, Q_u (N)	Increase in capacity (-)	capacity, Q_u (N)	Increase in capacity (-)
plain_T23	-	226.3	-	272	-	201.9	-	270.3	-
plain_T24	-	220.7	-	256.5	-	204.3	-	246.2	-
impression_T23	0.75	341.7	*1.51*	365.7	*1.34*	339.2	*1.68*	363	*1.34*
impression_T24	0.75	332.4	*1.51*	361.1	*1.41*	321.2	*1.57*	337.3	*1.37*
impression_T24	0.75	310.3	*1.41*	354.7	*1.38*	298.7	*1.46*	345.4	*1.4*

Table 5: Values of secant stiffness at selected settlement levels.

w/d	Resin Plain	Resin Impression	Plastic Plain	Plastic Impression	Ratio: Resin/Plastic Plain	Ratio: Resin/Plastic Impression
(-)	(N/mm)	(N/mm)	(N/mm)	(N/mm)	(-)	(-)
0.5%	1840 ±702	2002 ±306	1012 ±47	1762 ±124	1.82	1.14
1%	1296 ±332	1525 ±90	672 ±10	1133 ±113	1.93	1.35
2%	946 ±150	1095 ±35	396 ±21	686 ±80	2.39	1.60
5%	538 ±84	622 ±48	226 ±2	336 ±28	2.38	1.85

Table 6: Interface direct shear tests results.

Material	Shear stress s_u (kPa)	Peak stress, τ_p/s_u	Ultimate stress τ_u/s_u
clay	52.4	0.9	-
clay	57.2	0.93	0.68
clay	45.1	0.85	0.66
clay	53.8	0.91	0.7
resin	49.3	2.0	0.57
resin	55.1	3.25	0.57
precast resin	54.7	0.57	0.52
precast resin	48.9	0.50	0.47
plastic	42.7	0.38	0.33